Numerical modelling for reinforced concrete response to blast load: understanding the demands on material models

NUMERICAL MODELLING FOR REINFORCED CONCRETE RESPONSE TO BLAST LOAD: UNDERSTANDING THE DEMANDS ON MATERIAL MODELS

Jiaming Xu, Yong Lu*

Institute for Infrastructure and Environment, School of Engineering, The University of Edinburgh, The Kings Buildings, Edinburgh EH9 3JL, UK

* Correspondence: yong.lu@ed.ac.uk

Synopsis: Numerical modelling is nowadays commonly employed in the analysis of concrete structures subjected to extreme dynamic loadings such as blast. Sophisticated material models, particularly concrete, are available in commercial codes and they are often applied in their default settings in a diverse range of modelling applications. However, the mechanisms governing different load response scenarios can be characteristically different and as such the actual demands on specific aspects of a material model differ. It is therefore not surprising that a well-calibrated material model may exhibit satisfactory performance in many applications but behave unfavourably in certain other cases. Modelling the response of reinforced concrete structures to blast load presents such an important scenario in which the demands on the concrete material model are considerably different from high-pressure scenarios for example high-velocity impact or penetration. This paper stems from an initial modelling undertaking in association with the Blind Blast Contest organised by the ACI Committee 370, and extends to a detailed scrutiny of the demands on the concrete material model in terms of preserving a realistic representation of the tension/shear behaviour and the implications in a reinforced concrete response environment. Targeted modifications are proposed which demonstrate satisfactory results in terms of rectifying the identified shortcomings and ensuring more robust simulation of reinforced concrete response to blast loading.

Keywords: reinforced concrete, blast load, numerical simulation, concrete material model, damage mechanism, failure mode

Jiaming Xu is currently a PhD candidate at School of Engineering, The University of Edinburgh. His research topic involves numerical modelling of concrete materials and reinforced concrete structures under impact and blast loading.

Yong Lu is Professor and Chair of Structural Mechanics at The University of Edinburgh. His research interests include structures and structural materials under a variety of dynamic loads ranging from impact, blast to earthquakes. His research involves analytical, numerical as well as experimental studies. His more recent work has a focus on the micromechanical processes influencing the dynamic behaviour of concrete-like materials.

INTRODUCTION

The response of reinforced concrete (RC) structures to extreme dynamic loading such as blast and impact is complicated due to a combination of several factors, of widely cited ones being stress wave and strain rate (e.g. Bischoff and Perry[1]), inertia-induced confining effect (e.g. Donze et al.[2], Li and Meng[3], Song and Lu[4]), and large deformations. Extensive research has been devoted over the past decade or so to understanding each of these phenomena, and the research work has seen increasing involvement of the use of high fidelity numerical simulation techniques in more recent years. Indeed, numerical simulation has made it possible to scrutinise in great detail the development of the stress-strain fields and the evolution of damage during and after the transient phase of the blast effect. Sophisticated material models have been developed and continuously evaluated and calibrated to cater to the numerical simulation needs in a variety of dynamic loading conditions.

At the backdrop of all the developments it is worth pointing out that the response of a concrete structure or structural component subjected to a high impulsive load would invariably experience distinctive response phases from the initial contact with the incoming load to the later global deformation response. While the majority of the so-called hydrocode models for concrete-like materials have been validated to a varying extent in applications where high pressure and localised material response plays a dominant role in impact and penetration (e.g. Polanco-Loria et al.[5], Unosson and Nilsson[6]), near-field blast (e.g. Tu and Lu[7], Zakrisson et al.[8]), systematic examination of the performance of such material models extending into the global deformation phase is relatively limited. It is generally understood that the dominate mechanisms in the global deformation phase can be significantly different from those in the high-intensity transient local response phase; the fact that the pressure level becomes low in this phase of response requires the material model to be able to accommodate tension, shear, as well as the relatively simple compression behaviour under low pressure but still complex multi-axial stress condition. The demand on the material model being able to exhibit appropriate behaviour in tension and shear becomes particularly important in reinforced concrete structures to ensure that transfer of stresses between concrete and reinforcing bars can take place in a realistic “reinforced concrete” composite manner.

A numerical model for reinforced concrete that is capable of simulating the entire process from direct blast loading through to the final global deformation phase is generally required in civil engineering applications where the residual state and the residual capacities of the affected members can play an important role in the design and evaluation of such effects. However, as discussed above a concrete material model which has shown sound performance in high-intensity stress applications may not necessarily perform as well in a reinforced concrete environment under a global deformation scenario.

The recent blind blast contest organised by ACI Committee 370 provided an excellent and rather unique opportunities for an in-depth examination into the modelling of reinforced concrete response to blast loading with hydrocode material models. The test RC slab was reinforced by a single layer of steel bars without any shear links, and this reinforcement scheme poses high demands on the residual behaviour of the concrete model in tension and shear in maintaining an adequate degree of integration with the rebar, thus maximises the exposure of any issues of the concrete material model in this category of numerical simulation for RC structures.

This paper is mainly concerned about the behaviour of a representative concrete material model in hydrocode platform LS-DYNA[9], namely the Karagozian & Case Concrete Damage (KCC) model[10], when it is applied in modelling blast response involving global deformation. The main objectives are to demonstrate its performance under this regime of the responses, to investigate into the cause of some abnormal behaviour, and subsequently to propose and demonstrate possible remedies. For a comparison, another widely used model in LS-DYNA, the Continuous Surface Concrete (CSC) model[11], is also employed and discussed.

In the present paper, securitisation of the detailed response in relation to the basic behaviour of the material model suggests that the particular issue with the KCC model seems to originate from the abrupt descending of the material towards a zero strength state following a tension/shear dominated damage process, and the consequent diminish of the interaction between the steel rebar and the surrounding concrete. In contrast, the CSC

model always retains a certain level of residual capacity which enables an effective connection between the rebar and the surrounding concrete at the severely damaged but not completely failed state. However the CSC model tends to exhibit an overly ductile behaviour under a confined tension condition, which is also examined and discussed in this paper.

To rectify the behaviour of the KCC model towards the retention of a minimum level of residual tensile strength under large deformation, a modification to the default η-λ curve in conjunction with an adjustment to the compressive damage cumulative parameter b_1 in the KCC model is proposed. This modification scheme serves well the needs of providing a prolonged minimum level of tensile strength while avoiding unwanted alteration of the general compressive behaviour. The modification is demonstrated to improve the simulation using the KCC model remarkably and the modified results compare well with the relevant experimental results.

OVERVIEW AND GENERAL DISCUSSION OF THE CONCRETE MATERIAL MODELS

The concrete material models used in hydrocode simulation of the dynamic response under high rate loadings generally need to accommodate a wide range of pressure, stress states, strain rate, and levels of damage. Most of such material models are formulated in a similar damage plasticity framework. The KCC and CSC models employed in the present study, available in LS-DYNA, are well documented in previous publications[12-15] and have been subjected to extensive scrutiny and validation studies[7,12,16-19]. For the purpose of present discussion, an overview and discussion of some of the key features that relate closely to the behaviour in a typical reinforced concrete simulation environment is provided.

Strength surfaces and damage definition in KCC model

In KCC concrete model, three independent strength surfaces are defined for yield, maximum and residual strength, respectively. All these strength surfaces are pressure sensitive, and a complete definition requires eight material parameters which are determined from standard material tests[12]. At any state of damage, the prevailing strength surface is defined as a linear interpolation between the maximum and either the yielding or residual failure surfaces, depending on the cumulative damage level:

$$\Delta\sigma(=\sqrt{3J_2}) = \begin{cases} \eta\Delta\sigma_m + (1-\eta)\Delta\sigma_y & for \quad \lambda < \lambda_m \\ \eta\Delta\sigma_m + (1-\eta)\Delta\sigma_r & for \quad \lambda \geq \lambda_m \end{cases} \tag{1}$$

where $\Delta\sigma_m$, $\Delta\sigma_y$ and $\Delta\sigma_r$ represent the maximum, yielding and residual surfaces respectively. The interpolation factor η is a function of the modified effective plastic strain measure λ, as shown in **Fig. 1**, and it varies from 0 (before yielding) to 1 (when λ equals to λ_m) to allow the strength surface to move between yielding to the maximum strength surface, then from 1 to zero to allow softening to develop between the maximum and residual surfaces.

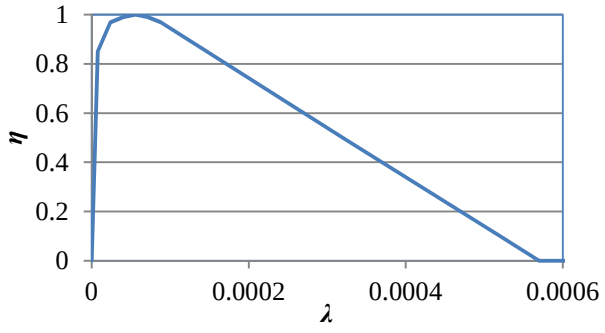

Fig. 1 - The default η-λ curve defined in KCC model

The modified effective plastic strain λ is defined as

$$\lambda = \begin{cases} \int_0^{\overline{\varepsilon^p}} \dfrac{d\overline{\varepsilon^p}}{r_f\,(1+p/r_f\,f_t)^{b_1}} & for \quad p \geq 0 \\ \int_0^{\overline{\varepsilon^p}} \dfrac{d\overline{\varepsilon^p}}{r_f\,(1+p/r_f\,f_t)^{b_2}} & for \quad p < 0 \end{cases} \tag{2}$$

where the effective plastic strain increment is given by

$$\overline{\varepsilon^p} = \sqrt{(2/3)\varepsilon_{ij}^p \varepsilon_{ij}^p} \tag{3}$$

f_t, r_f and ε_{ij}^p are the tensile strength, rate scaling factor and total plastic strain component, respectively. b_1 and b_2 are exponential weighting factors to control different rate of accumulation of incremental plastic strain in the hydrostatic compression ($p \geq 0$) and tension regime ($p < 0$), and in this way the softening phase develops in distinctive manners under compression and tension, respectively, while the same η-λ curve is employed.

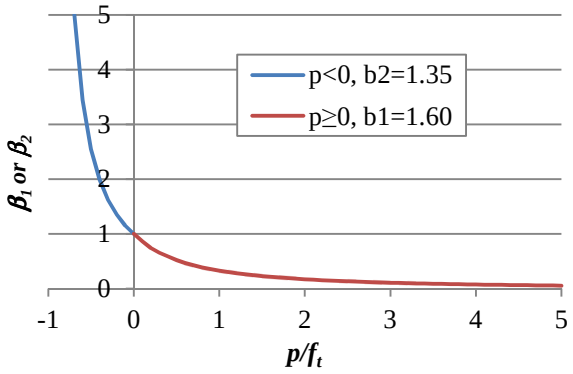

Fig.2 - Incremental plastic strain multiplier vs. hydrostatic pressure

For an illustrative purpose, let the rate scaling factor be unity (no strain rate effect) and the multiplier of the incremental plastic strain in **Eq.2** may be written as:

$$d\lambda = \begin{cases} (\beta_1)\overline{d\varepsilon^p} & for \quad p \geq 0 \\ (\beta_2)\overline{d\varepsilon^p} & for \quad p < 0 \end{cases} \tag{4}$$

where $\beta_1 = \dfrac{1}{(1+p/f_t)^{b_1}}$, $\beta_2 = \dfrac{1}{(1+p/f_t)^{b_2}}$.

With KCC default values of b_1=1.6 and b_2=1.35, the variation of β_1 and β_2 with pressure are plotted in **Fig. 2**. It can be seen that with the default b_1 and b_2 values, the rate of damage accumulation is greatly accelerated in negative pressure regime and decelerated in positive pressure regime and a smooth transition is enabled at zero pressure point.

It is also noted that the actual values of b_1 and b_2 themselves control the rate of accumulation of the incremental plastic strain into the total λ, thus different shapes (slopes) of the softening branch may be realised by adjusting the b_1 (for compression) and b_2 (for tension) values.

In the KCC model, the damage level is directly related to the modified effective plastic strain. For post-processing purpose, a damage scalar called SDF (scaled damage factor) is further introduced and it is defined as follows:

$$SDF = \frac{2\lambda}{\lambda + \lambda_m} \tag{5}$$

As λ is a positive non-decreasing variable, SDF varies from 0 to 2. In the pre-peak phase 0<SDF<1, and when concrete enters softening phase, 1<SDF<2. SDF eventually approaches 2 as λ increases to infinity, which ultimately represents a total damage state. A more detailed look into the variation of SDF with the accumulation

of damage will be given later in comparison with the damage index adopted in the CSC model.

Strength surfaces and damage definition in CSC model

The failure surface in CSC model is defined as a smooth intersection between a shear failure surface $F_f\left(I_1\right)$ and hardening cap $F_c\left(J_1,\kappa\right)$, as expressed in **Eq.6**.

$$f\left(I_1,J_2,J_3,\kappa\right)=J_2-\Re^2F_fF_c \tag{6}$$

With failure surfaces defined above, the model uses a scalar damage index d to transform the undamaged stress tensor into damaged one:

$$\sigma_{ij}^{damaged}=(1-d)\sigma_{ij}^{damaged} \tag{7}$$

Damage index d ranges from 0 for no damage to 1 for complete failure, and is defined in accordance with two strain-based energy terms, namely, brittle and ductile damage index d_b and d_d for tensile and compressive stress state respectively,

$$d=\begin{cases}\max(d_b,d_d) & p<0\\ d_d & p>0\end{cases} \tag{8}$$

To simulate the crack opening and closure, the brittle damage index drops to zero whenever the hydrostatic pressure enters compression, such that the residual compressive strength and stiffness is recovered as crack closes. Once the pressure switches from compressive to tensile again, the previous maximum value of the brittle damage index is reactivated. The softening function of d_b and d_d are defined as a function of the damage threshold τ, which is a term used to describe the current strain and energy accumulation,

$$\begin{aligned}d_b&=\frac{1}{D}\left[\frac{1+D}{1+D\exp^{-C\tau b}}-1\right]\\ d_d&=\frac{d_{\max}}{D}\left[\frac{1+B}{1+B\exp^{-A\tau d}}-1\right]\end{aligned} \tag{9}$$

Parameter A, B, C and D control the shape of the softening function. The brittle damage threshold τ_b is defined by the maximum principal strain, whereas the ductile damage threshold τ_d depends on the total strain components, as follows:

$$\begin{aligned}\tau_b&=\sqrt{E\varepsilon_{\max}^2}\\ \tau_d&=\sqrt{\frac{1}{2}\sigma_{ij}\varepsilon_{ij}}\end{aligned} \tag{10}$$

Consideration of fracture energy and mesh convergence

The general considerations of crack softening in both KCC and CSC models stem from the crack band theory[20]. To enable a mesh-objective solution and general mesh convergence, both KCC and CSC models essentially incorporate a length factor, albeit in a different manner, which relates the strain energy over a characteristic "band width", L_c, in the softening phase of the material response to target fracture energy, G_f, which is considered as a material property[21]. In a general form, this requirement transpires to satisfying the condition expressed in **Eq.11**:

$$\int_{\varepsilon_m}^{+\infty}\sigma d\varepsilon=\frac{G_f}{L_c} \tag{11a}$$

or

$$\int_{\varepsilon_m}^{+\infty}\sigma(L_c d\varepsilon)=\int_{\delta_m}^{+\infty}\sigma d\delta=G_f \tag{11b}$$

In CSC model, L_c is simply tied to the characteristic element size L_e (cubic root of the element volume), implying that the softening (crack) is always localised within a single layer of elements. On the other hand, KCC model provides a possibility of dealing with softening to spread (in the band width direction) over multiple elements, and this is achieved by introducing a user specified localisation width L_w. When the element size L_e is larger than L_w, the standard treatment prevails such that the characteristic length L_c in **Eq.11a** is made equal to the element size L_e. In case the element size is smaller than L_w, the stress-strain relation is then adjusted based on

the assumption that the facture energy is dissipated within the localisation width L_w rather than a single element length L_e. In short, the handling of the softening and consideration of the strain energy through a characteristic band width in KCC and CSC may be summarised in **Eq.12**:

$$L_c = \begin{cases} L_e & for \quad CSC \\ \max(L_e, L_w) & for \quad KCC \end{cases} \tag{12}$$

For FE analysis in relatively simple tension-dominated loading conditions, localisation will inevitably occur along a single row of elements perpendicular to the primary tension direction. In such situations it is obvious that the localisation width should be tied to the element size, which means L_w should be given a value equal to the characteristic element size L_e. However when the stress state becomes complicated in a damage zone, the localisation width could spread across more than one element in the FE model, particularly in the case of a refined mesh, and consequently the setting of L_w would become a complicated issue and an appropriate choice could be case-dependent. Further discussion along this line is beyond the scope of this paper. In the present calculations, the standard option that the target fracture energy is realised over a single element width is adopted.

Further discussion on interpretation of the damage indices

In view of the different ways that the damage scalars are defined in the KCC and CSC models (similarly in other damage plasticity models), single-element numerical tests are conducted to demonstrate the concrete response and the computed values of damage under uniaxial tension and compression. A single cubic element with a length of 25.4mm (1in) and compressive strength of 30MPa (4.35ksi) is chosen.

The uniaxial tension and compression stress-strain curves produced from the KCC and CSC models, respectively, are shown in **Fig. 3** along with the indication of the damage scalar values. Note that the absolute strain values in a single element test is element-size dependent, as can be understood from **Eq. 4**, so the strain values need to be read with the element size in mind. On the other hand, the total deformation of the element, which in the tension case would represent the "crack width", would be independent of the element size. The scale of deformation values are also indicated on the top axis in **Fig. 3**.

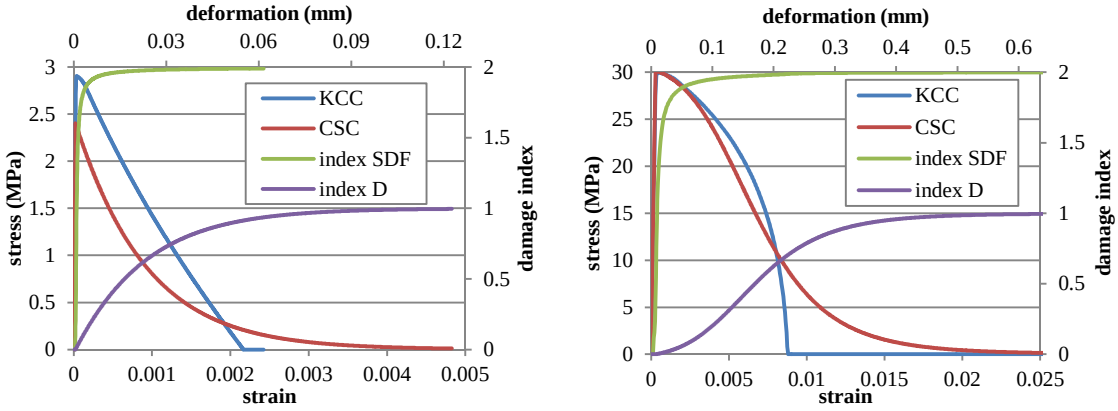

a) uniaxial tension b) uniaxial compression

*Fig. 3 - Uniaxial stress-strain curves produced by the two material models (1mm=3.94*10^{-2}in)*

From **Fig. 3** it can be seen that slight difference in the tensile strength exists between the two models for the same target compressive strength. More remarkably, however, the shapes of the softening curves are different in characteristics. Taking the tensile curves for example, while both KCC and CSC curves tend to cover a similar area (thus indicating similar fracture energy), the KCC model has a terminate strength cut-off at a strain level of about 2.3*10^{-3}, or a "crack width" level of about 0.06mm (2.3*10^{-3}in), beyond which the material would have zero strength. On the contrary, the CSC model has a more gradual descending phase. The patterns of the curves in compression are similar to the respective tensile curves. Further discussion about the potential effect of the KCC model having a strength termination point will be given later.

With regard to the damage scalars, aside from the fact that the SDF factor in KCC has a scale range of 0~2 while the damage index in CSC has a range of 0~1, which may be unified easily if needed, the SDF factor tends to exhibit a narrow effective range as it is already greater than 1.5 before reaching the maximum strength. In comparison, the damage index in CSC model tends to exhibit a more gradual increase while the material softening accumulates. The D index appears to closely relate to the (descending) stress state and the absolute strain, which seems to be physically more meaningful.

Fig. 4 further illustrates the relationship between the SDF and D indices. Form the whole range perspective, the two indices do not appear to get along with each other. But upon a loser look, they are reasonably correlated in the medium to severe damage states. In the D index case, this marks a range of 0.3 to 1.0, but the corresponding SDF is in a very narrow range of 1.97~2.0. This effective range of the SDF values for severe material damage needs be particularly noted when it comes to interpreting the severe damage or crack patterns with the SDF factor.

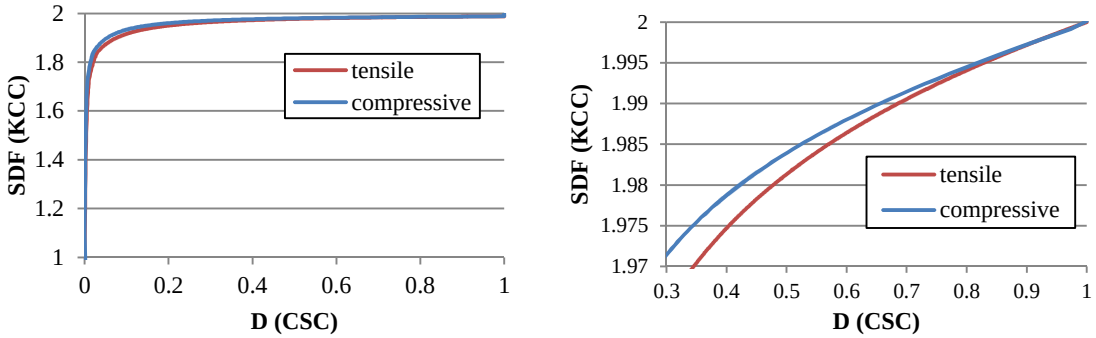

Fig. 4 - Relationship between SDF in KCC and D in CSC model

NUMERICAL SIMULATIONS AND COMPARISON WITH EXPERIMENTAL RESULTS

The motivation of the present investigation into the performance of concrete material models in a reinforced concrete structure stems from the initial experiences acquired from the numerical simulation exercise in connection with the Blind Blast Contest[22]. Full details of the physical experiments were not available at that time but exploratory simulations[23] using KCC model demonstrated some unexpected abnormal response as compared with the simulation using the CSC model. The overall structural response in such a loading scenario was primarily of a monotonic process, and consequently the performance of these material models was expected not to differ significantly. However, it has been discovered, rather surprisingly, that the KCC model could not produce a sensible result especially in the later stage of the response, whereas the CSC model exhibits reasonable performance throughout the entire response.

In this section, the simulation of the RC slab is introduced and discussed in light of the experimental results that have now been made available[24]. The abnormal response in the KCC model is highlighted. The numerical investigation is then extended to the simulation of a quasi-static RC beam test to further observe the material model response without the involvement of possible dynamic effects, and furthermore to the simulation of a concrete pull-out test scenario to ascertain the identification of the cause of the problems.

Simulation of RC slab response to blast load

The simulation being discussed here is concerned with the normal strength RC slab in the contest programme. The RC slab, along with other specimens, was originally tested at the University of Missouri Kansas City (UMKC) using a blast loading simulator, which is capable of simulating a uniform pressure pulse on the loading face. The slab was supported against two strong steel box beams on the rear side of the slab, and the response of the slab was measured by accelerometers and laser measurement device attached to the rear face of the slab. The test RC slab was a one-way slab with a net span of 1320 mm (52in) and a thickness of 101.6 mm (4in). The longitudinal reinforcement consisted of 9 No. 3 steel bars of diameter 9.525mm (3/8in), and nominal transverse reinforcement consisted of 5 No. 3 steel bars. All the reinforcing bars were placed on the bottom side (opposite to the loading face) of the slab. The normal strength RC slab was cast using concrete with a compressive strength of 34.5 MPa (5ksi). The reinforcing bars were of Grade 60(ksi).

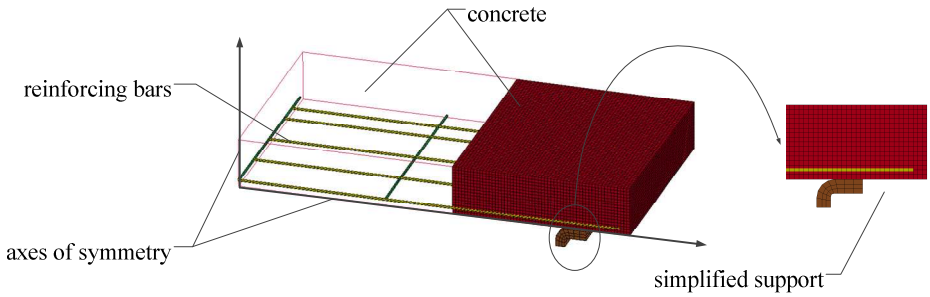

Fig. 5 - Layout of the ¼ FE model for the slab and the end support beam

The numerical simulation is carried out using LS-DYNA. In the FE model for the slab, 8-node solid elements are used for concrete whilst 2-node beam elements are used for longitudinal and transverse reinforcements. The rebar elements are embedded in the solid elements such that they connect to the concrete elements with shared nodes, mimicking a perfect bond condition. To preserve the support condition, the profile of the support box beam was retained in the model and the RC slab is placed on the support beam via surface to surface contact. Considering the symmetry, only ¼ of the test RC slab needs to be modelled, as depicted in **Fig. 5**.

The concrete in the RC slab is modelled by KCC and CSC material models in two different FE models, respectively. In both models, the automatic generation of material model parameters is adopted by specifying only the unconfined compressive strength, which is 34.5MPa (5ksi) based on the experimental data. A mesh convergence study was conducted and according the results a nominal mesh grid size of 6.35mm (1/4in) was adopted in both FE models for the detailed simulations. This offers a resolution of 16 solid elements along the slab thickness, with a total of about 140,000 elements. Correspondingly, a localisation width (L_w) of 6.35mm (equal the average element size) is employed in the KCC model.

In the FE model, the rebar elements are modelled by the material model *MAT_PIECEWISE_LINEAR_PLASTICITY, which allows a piece-wise definition of the stress-strain relationship to match closely the actual post peak stage of the test result. Blast load is simulated by uniformly distributed pressure pulse onto the loading face of the RC slab, using the pressure history recorded from the actual experiment.

Fig. 6 shows the time histories of the central deflections and reaction forces in the ¼ models using KCC and CSC model, respectively. The experimental blast force is calculated based on the pressure pulse applied onto the one-quarter model of the slab.

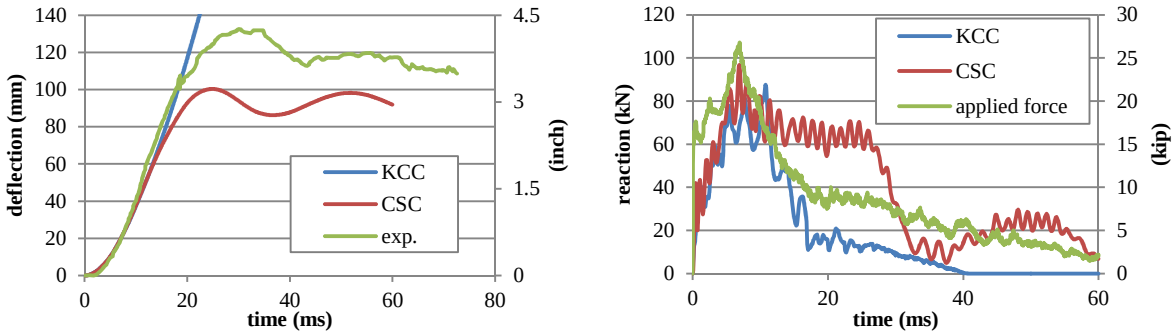

Fig. 6 - Time history of central deflection and reaction

As can be seen from **Fig 6**, the deflection predicted by the CSC model agree well with the experimental results, and it exhibits an increasing phase until about 100mm (3.9in or 7.6 % of the span), followed by a stable oscillation around a permanent plastic deformation, as observed from the actual experiment. In contrast, the deflection time history from the KCC model shows an unstable (diverging) response following the initial increase of the deflection. It is noteworthy that the slab appears to have failed globally in the KCC model at about 13ms when a central deflection reaches only about 60 mm (2.4in or 4.5% of the net span), which is well below the peak deflection experienced in the experiment.

Fig. 7 shows the damage patterns along the rebar and over the slab depth at selected time instants as obtained using the KCC (left) and CSC model (right). The final crack patterns of the experimental RC slab, as reported in ref[24], are reproduced in **Fig. 8** for a comparison. Note that in order to make the damage comparable, the scale of the SDF in KCC model is narrowed to a range of 1.97~2.00 against a range of 0.3~1.0 in CSC model in

accordance with the calibration results shown earlier.

It can be observed from both KCC and CSC models that at the initial stage, damage develops as bending cracks, starting from the mid-span region and then propagating towards the support. However, upon reaching the peak resistance at around 10 ms, the model with KCC concrete exhibits a rapid spread of damage in concrete surrounding the longitudinal reinforcing bars and in the high shear region. The spread of failure in concrete in the KCC model appears to eventually result in the longitudinal rebar detaching from the surrounding concrete alongside loss of shear capacity over the depth of the slab at about 14 ms, leading to a complete loss of the global resistance of the slab.

In contrast, the damage in the model with CSC tends to stabilise with a final crack pattern featured by distributed lateral cracks together with longitudinal cracks along the main reinforcing bars, which agree favourably with the experimental result.

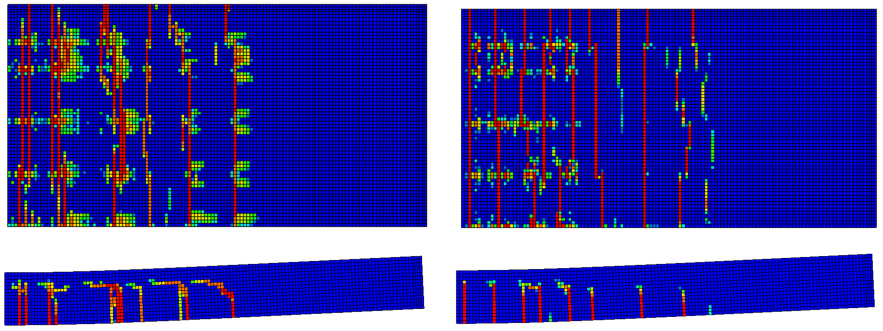

t=8ms

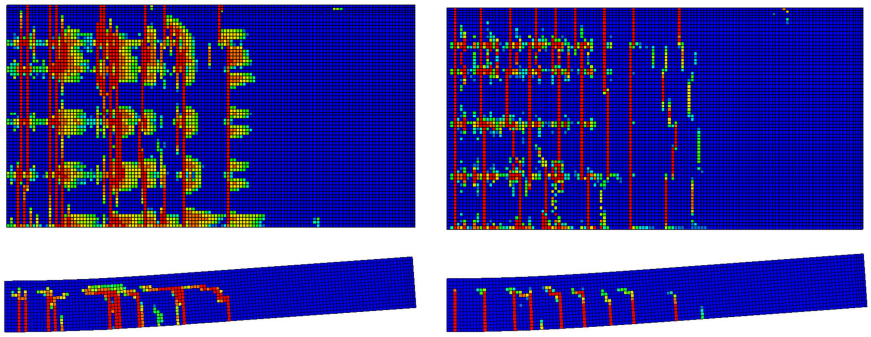

t=10ms

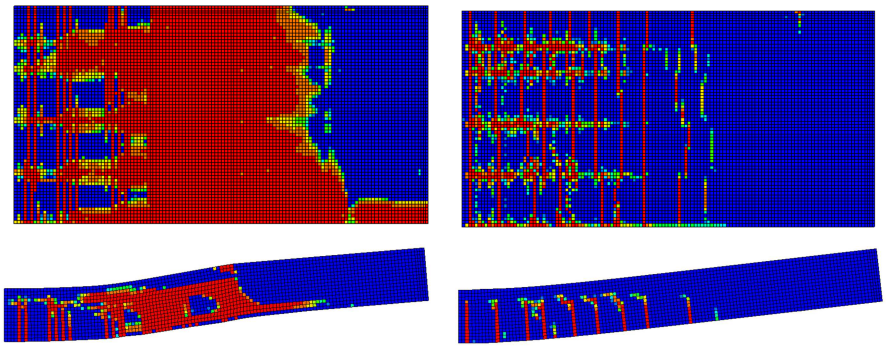

t=14ms

(left: KCC_1.97~2.00; right: CSC_0.3~1.00)

Fig. 7 - Damage distribution in the slab surface and over cross-section

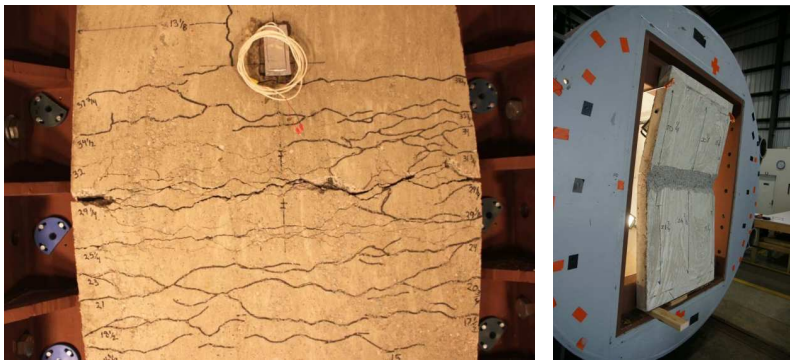

Fig. 8 - Experimental crack distribution after blast (courtesy from ref [22,24])

Fig. 9 presents the evolution of the axial stress distribution in rebar at selected time instants. At the early stage of the response up to about 8 ms, the axial stress in the rebar develops in a similar fashion in both KCC and CSC models, and is consistent with a flexure-controlled response under a distributed load. The shear-bond stress in the concrete elements to which the rebar elements are attached is correlated to the slope of the longitudinal distribution of the axial stress in the rebar. From **Fig. 9** it can be observed that when the global response reaches a certain limit, herein at about 10ms, the stress in the rebar stops increasing in the KCC model, indicating that the shear and the rebar anchorage region (closer to the end support) starts failing, while displacement increases uncontrollably.

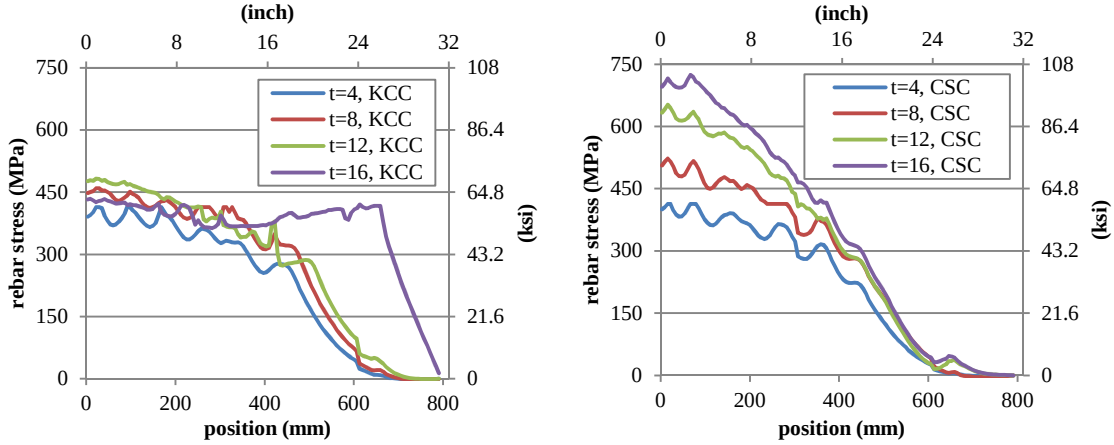

Fig. 9 - Development of axial stress distribution along longitudinal rebar (t: ms)

Comparing to the KCC model, the axial stress in the CSC model exhibits a consistent but globally increasing pattern as the response develops to reach the peak deformation. There is no sign of extensive bond or shear failure in the concrete. Further details about the comparative simulations between the two models for the RC slab can be found in ref[23].

Simulation of RC beam under quasi-static load

In recognition of the fact that the significant differences in the simulation results between the two models occur in the global deformation phase of the response, and in particular the KCC model appears to exhibit a premature global failure, it was considered useful to carry out a simulation on a static RC beam to further examine the material behaviour in a global deformation mode of response, but without any transient dynamic influences.

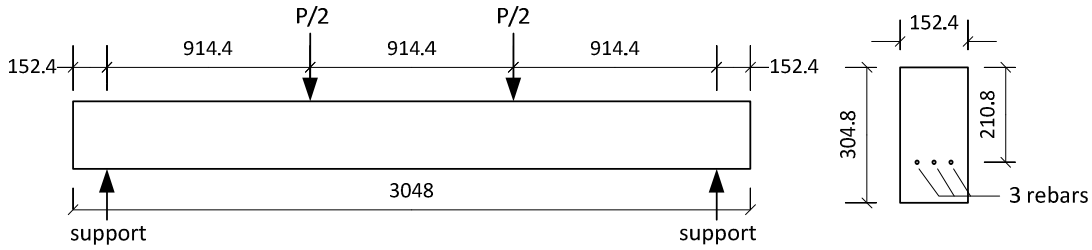

(a) Dimensions of specimen (unit: mm, 1mm=3.94*10-2in, adapted from ref25)

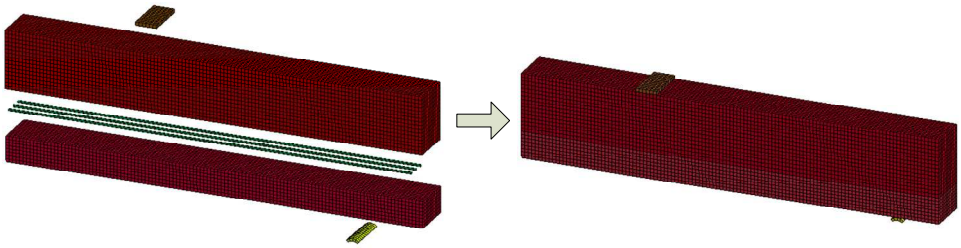

(b) Geometric layout of numerical model

Fig. 10 - Experimental RC beam and its FE model

As mentioned before, to fully expose the behaviour of the concrete material model in interacting with the main reinforcing bars, it is desirable that the RC specimen involves only a simple layer of main reinforcing bars. For this reason, the RC beam tests conducted by Janney[25] are selected. The particular test beam considered for the present simulation is shown in **Fig. 10(a)**. The beam had a net span of 2743mm (108in), it had only longitudinal reinforcement without any stirrups. The longitudinal reinforcement consisted of 3 No. 5 steel bars giving rise to a reinforcement ratio of 1.87%. The beam was tested in a four point-load bending configuration. The length to thickness ratio was about 13, similar to the RC slab presented earlier. The concrete used in the test beam had a compressive strength of 36.2 MPa (5.25ksi) with tensile strength assumed to be 2.82 MPa (0.111ksi), and the reinforcing bars had an yield strength of 333 MPa (48.3ksi).

As reported in experiment[25], the beam developed about five cracks in the region of pure flexure. After yielding occurred in the tension rebars, the flexural deformation developed in a ductile manner without much increase of the loading capacity. Finally the beam failed in a flexural mode without any apparent shear or bond problem.

Similar FE model set-up as used in the simulation of the RC slab is employed here, as depicted in **Fig.10(b)**. The steel bars are modelled by beam elements while concrete is modelled by solid elements. Concrete model parameters are generated automatically for the 36.2MPa (5.25ksi) class concrete. According to experimental observation[25] no apparent hardening stage existed in the stress-strain relation of the steel bars thus the rebar is assumed to be elasto-plastic in the numerical model.

A mesh convergence study was conducted to identify an acceptable mesh size while maintaining a manageable computational time, which is generally much longer due to the test being quasi-static. Finally an average element length of 6.35mm (1/4in) is chosen for the beam simulation using both the KCC and CSC models.

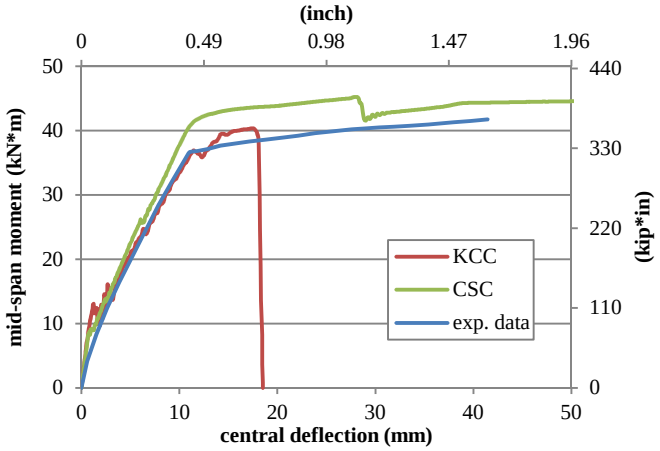

Fig. 11 Comparison of central deflection – mid-span moment curves

The predicted load (mid-span moment) vs. central deflection relationships using the two models are compared with the experimental result in **Fig. 11**. It can be clearly observed that the results generally repeat what have been observed in the RC slab blast simulation shown in **Fig. 7**. For the particular RC beam herein with no shear links or stirrups, the KCC model tends to fail prematurely with an abrupt loss of the global resistance at a deflection of 18mm (0.71in or approximately 1/150 of the net span). On the other hand, the CSC model appears to match well the experimental curve with a slightly higher strength. It is noted that the experimental failure point was recorded at around 42mm (1.65in).

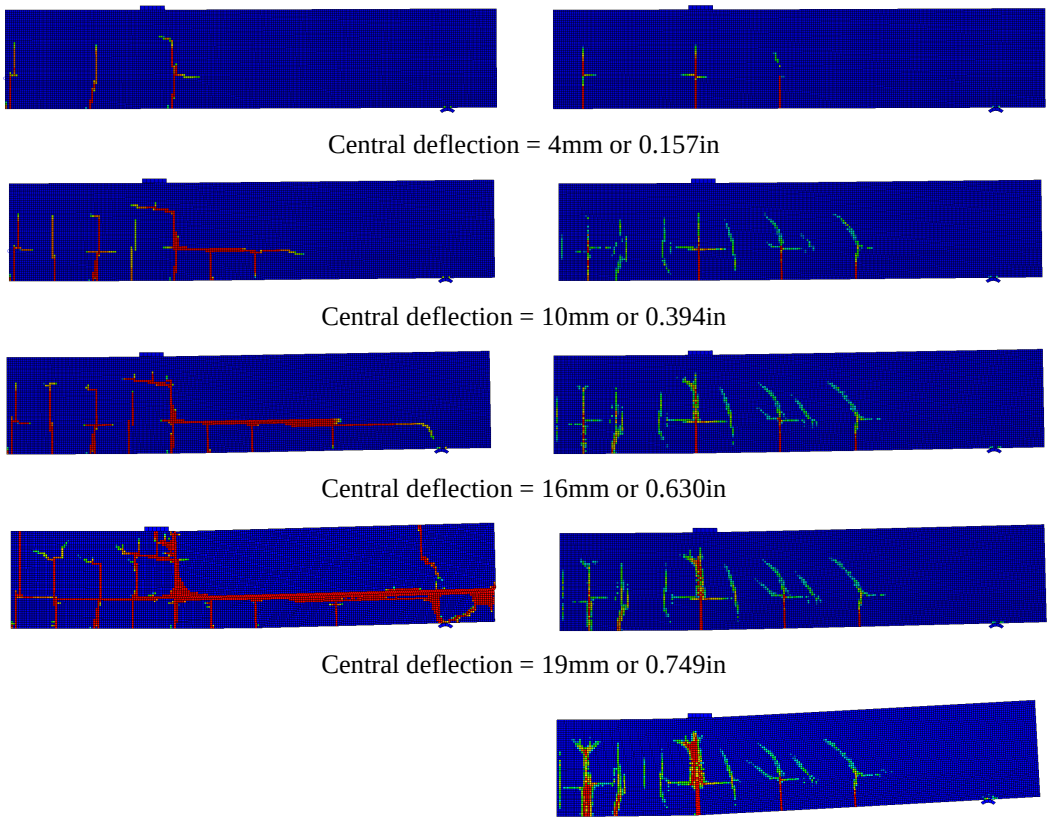

Fig. 12 Damage pattern of RC beam under quasi-static load (left: KCC_1.97~2.00; right: CSC_0.35~1.0)

The development of the damage (crack) patterns at selected deflection levels are shown in **Fig. 12**. The failure pattern in the KCC model also suggests that the premature and abrupt failure in this model is attributable to the failure of concrete elements to which the rebar elements are attached in the high shear/anchorage region (between the point load and the support), essentially resulting in the loss of the reinfrocement effect (analyguous to the rebar being pulled out or sliding in the concrete). The CSC model also developed damage along the longitudinal rebar but the effect is not catastrophic and the overall behaviour matches well the experiment as mentioned earlier.

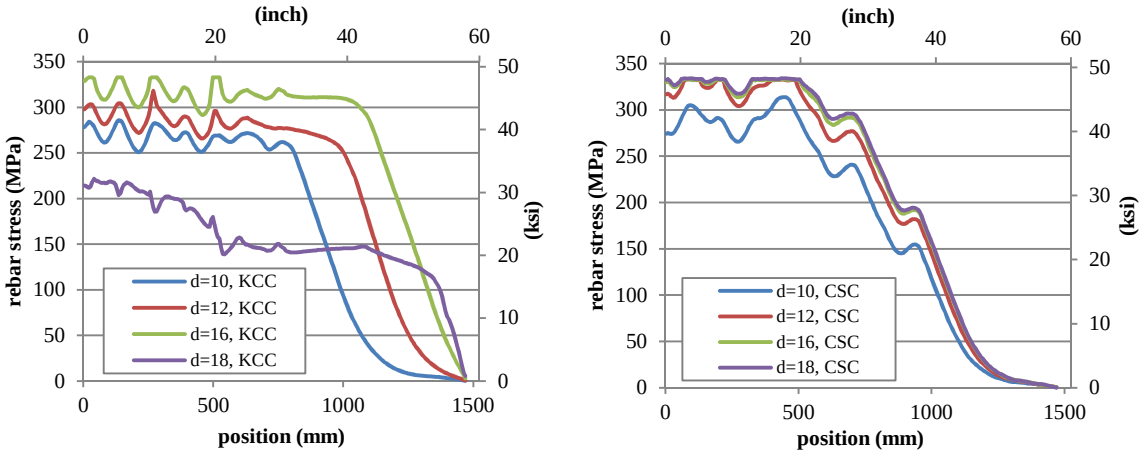

*Fig. 13 Axial stress distribution along the length of rebar (d: mm, 1mm=3.94*10^{-2}in)*

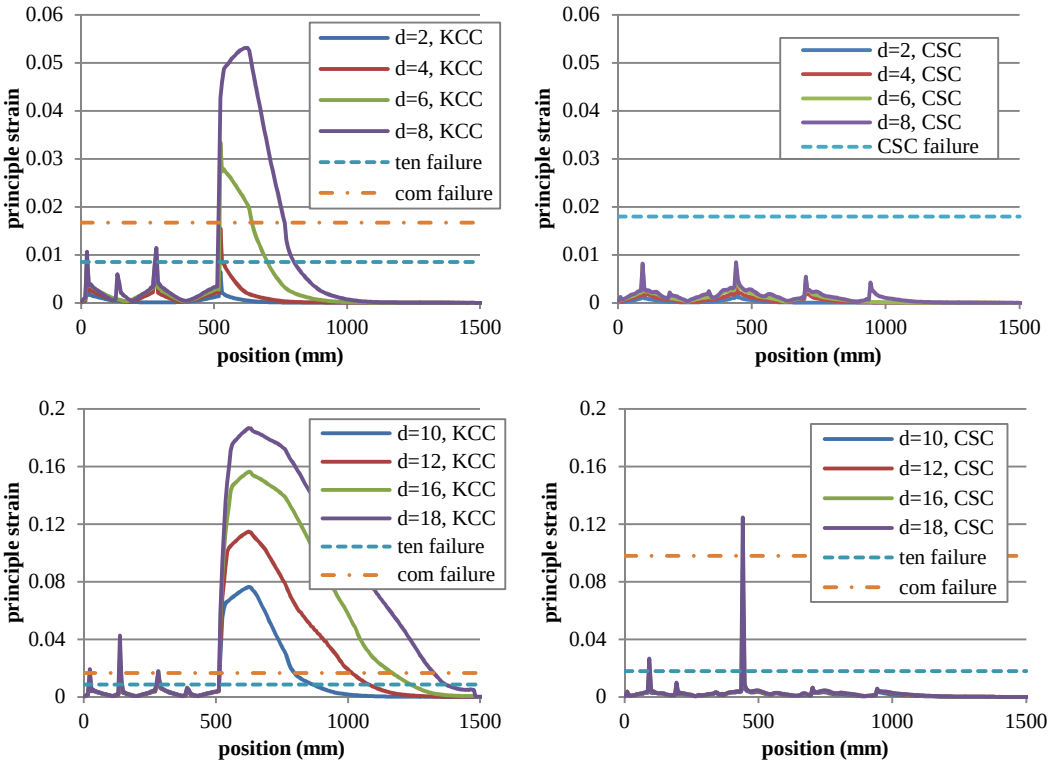

*Fig. 14 Principle strain in concrete elements connected to rebar (d: mm, 1mm=3.94*10^{-2}in)*

In a closer inspection at the failure process of rebar and concrete interaction, the evolution of axial stress distribution in rebar, together with the principle strain (tensile positive) in the concrete elements connected to the rebar at selected deflection levels are presented in **Fig. 13** and **14**, respectively. The correspondent strain limits at which the KCC/CSC model would completely lose its strength under uniaxial tension and compression are also shown as a benchmark. It can be seen from the model with KCC that as early as a deflection of 4mm (0.157in), strain begins to increase drastically at the flexural crack 500mm (19.7in) from the mid-span. It immediately exceeds the strain limit and becomes stress-less, and results essentially in the loss of stress transfer between the concrete and the rebar at this point. This renders an accelerated spread of "bond" failure in the shear span towards the support. When the global response reaches 18mm (0.709in), almost the entire set of the concrete in the shear span exceeds the total failure strain limit and becomes "stress-less" in the KCC model.

Comparing to KCC model, the strain in the concrete connected to the rebar develops considerably below the strain limit in CSC model, thus no significant connection failure takes place and the axial stress in the rebar exhibits a consistent but globally increasing pattern as the beam deflects.

Further examination of the concrete models in a pull-out setting

The issues with the interaction between rebar and concrete identified in the KCC models is further examined in a direct pull-out setting. The classical pull-out tests conducted by Eligehausen[26-27] are modelled.

The test specimen, which represented the confined region of a typical beam-column joint, was around 300mm by 180mm by 380mm (12in by 7in by 12in) and casted by 30MPa (1.18ksi) concrete. The size of longitudinal rebar was Grade 60, #8 (25.4mm or 1in), with secondary stirrups consisted of #4 (12.7mm or 0.5in) bars. Only a short bond length of 5 times of rebar diameter was created in the test specimen. Load was applied using a displacement controlled procedure such that the scheduled development of slip was achieved. The net slip was measured at the unloaded bar end.

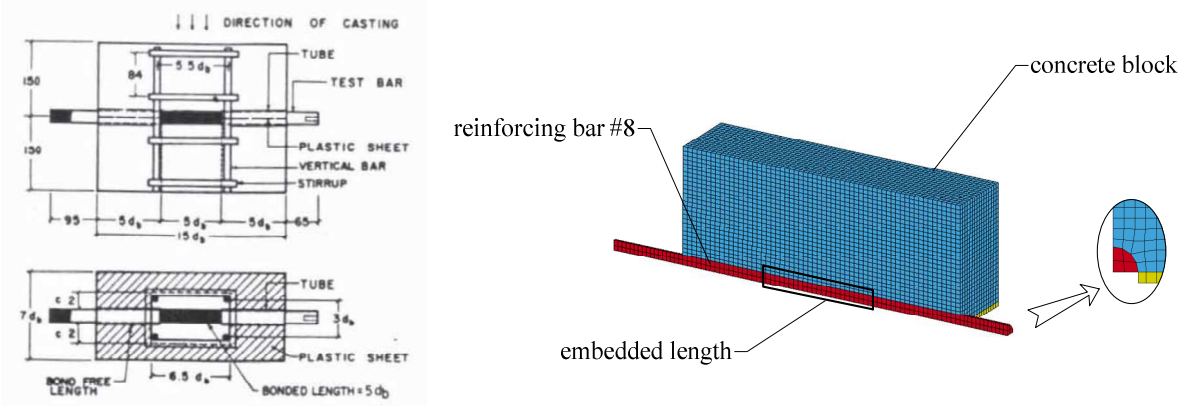

Fig. 15 Test specimen[26] and numerical model setup

For the present verification purpose, only the specimen without stirrups is simulated. Considering the symmetry, one-quarter the specimen is modelled. Concrete and longitudinal rebar are all simulated by solid elements, as shown in **Fig. 15**. In the numerical simulation load is also applied at one end of the longitudinal rebar in a displacement controlled manner. Due to the explicit scheme used in the analysis, the rate of applying the displacement was made sufficiently slow (10mm per second) to avoid any unwanted transient effect while at the same time avoid excessive computational time.

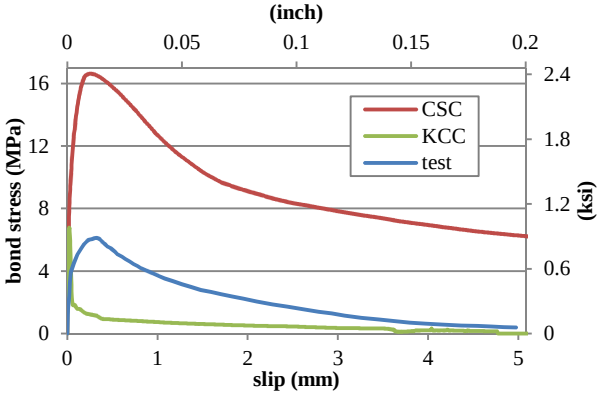

Fig. 16 Comparison of global bond-slip relation

Fig. 16 shows a comparison of the simulated bond stress-strain curves using the KCC and CSC models, respectively, in comparison with the experimental curve. Clearly, the KCC model exhibits again overly brittle bond-shear behaviour and the specimen fails rather steeply when the maximum bond stress was attained. This observation is consistent with the results from the RC slab and beam simulations presented in the previous sections. It is noteworthy that the CSC model, while still withholds a reasonable trend in the overall behaviour, tends to overpredict significantly the bond strength as well as the overall slip deformability. This phenomenon with the CSC model that has not become apparent in the RC slab and beam simulations, and it in fact exposes a potential pithole of this particular model when it comes to situations involving tension or shear under a confined (hydrostatitc pressure) stress conditions. A further note on such behaviour of the CSC model will be given later.

PROPOSED MODIFICATION TO THE STANDARD KCC MODEL

General discussion of the modification strategy

The extensive analysis of the failure processes in the simulated results reveal that the global failure in the RC members with the KCC model tends to be premature, and this phenomenon is deemed to be resulting from a premature and complete loss of “bond” strength in the concrete elements surrounding the rebar. The premature failure of these concrete elements will equate elimination of the reinforcement effect, leading to a premature collapse of the RC member as if it was un-reinforced in the late stage of the response.

The concrete elements surrounding the rebar are generally in shear and tension dominated stress state, whether or not involving certain amount of hydrostatic pressure. Therefore it would be rational to seek rectification by prolonging the softening or descending phase of the material response under tension and avoiding the material

entering zero strength prematurely. The ability to maintain a minimum level of resistance can be particularly important to KCC like models that adopt an isodamage approach in which a concrete element failed completely in tension would not possess any strength when the stress condition is reverted to compression. This aspect may have played a certain role in the observed premature global failure in the RC slab and beam simulations.

The above objective of achieving a more gradual softening and avoiding early attainment of a zero strength state may be achieved via modification to the relevant material model formulation. In the existing implementation of the KCC model in LS-DYNA, however, such effect may be realised by modifying the damage accumulation curve (the η -λ curve) together with an adjustment of the plastic strain weighting factors.

Modifications to the softening parameters in KCC model

As discussed earlier, in KCC model the damage accumulation or softening rate are controlled by the η-λ curve in conjunction with the exponential factor b_1 and b_2 in a comprehensive manner. In particular, the η-λ curve affects directly the shape of softening curve, whereas the factor b_1 and b_2 control the rate of damage accumulation under tension and compression respectively, based on the equivalent plastic strain. In combination these parameters give rise to a desired softening stress-strain relation and guarantee a certain fracture energy level. It should be noted that the determination of the fracture energy for concrete is still a subject of continued study and for the same type of concrete the variation range of the fracture energy could be rather significant. For this reason, in the present proposal of modifying the softening behaviour of the KCC model we do not confine ourselves to a specific fracture energy; however the same modification approach can still be applied as one wishes for the fracture energy to be kept constant for different softening behaviours.

As demonstrated earlier, the default η-λ relation, which is basically a linear function, generates a uniaxial stress-strain curve with a very steep softening response under both uniaxial tension and compression, with a clear strain (or deformation) limit beyond which the strength will become and remain zero. A more gradual accumulation of the damage, and hence the more gradual softening and delayed elimination or a minimum strength, may be achieved by modifying the second branch of the η-λ function into an exponential form.

Based on above considerations, a set of the exponential functions with a different termination limit of the λ_{max} values, as shown in **Fig. 17**, are proposed to yield different degrees of gradual softening behaviours and retain a certain level of residual strength at a certain softening strain range.

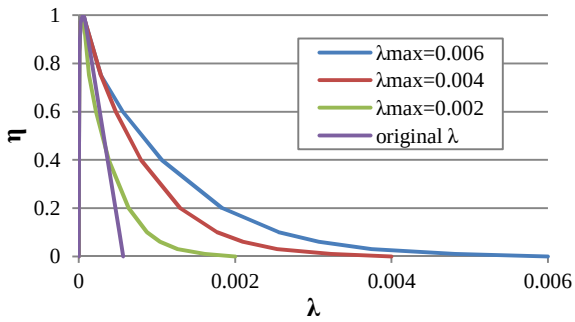

Fig. 17 Modified η-λ curve

As also discussed earlier, in KCC model the same η-λ is used for both tension and compression regimes, and different softening features in compression and tension are controlled by the plastic strain accumulation factor b_1 and b_2 respectively. Now that the η-λ curve is modified with an explicit aim to achieve a gradual softening in tension but not so much in compression, as far as the problems under the present investigation are concerned, the b_1 factor, which takes effect when the stress conditions comes into the (hydrostatic) compression regime, will need to be adjusted accordingly so as to compensate (depress) the unwanted stretching of the softening behaviour in the general compression region due to the prolonged η-λ curve.

Parameterisation of η-λ curve and b_1 factor

The responses of single element using modified KCC model with different lambda limits, under varied load conditions, namely uniaxial tension and uniaxial compression, are given in **Fig. 18**. Inlcuded in **Fig. 18** is also the behaviour of the element under a confined tension, which is identified to be a representative stress state in the concrete elements surrounding the rebar.

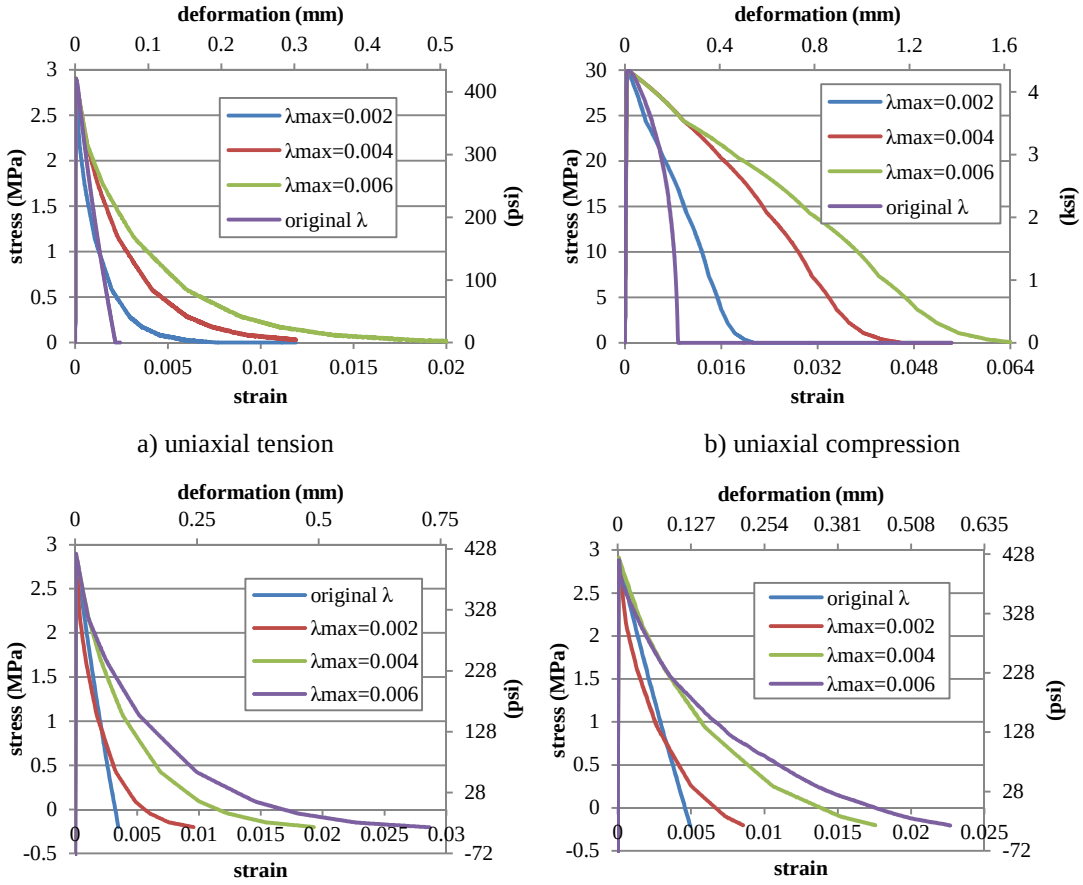

a) uniaxial tension

b) uniaxial compression

c) confined tension (1.5MPa)

d) confined tension (3MPa)

*Fig. 18 Influence of η-λ curve on stress-strain curves (element size = 25.4mm, 1mm=3.94*10^{-2}in)*

It can be immediately observed that the softening branch of the uniaxial tension is markedly affected by the modification of the η-λ function and softening becomes increasingly gradual as the limiting value of λ_{max} is increased, and this effect also holds in the two examples of confined tension scenarios. However, as mentioned in previous paragraph the effect from the modified η-λ curve carries over to affect the compressive stress-strain relationship as well, making the material unrealistically ductile in compression as can be seen from **Fig. 18(b)**.

The compressive plastic strain factor b_1 is therefore adjusted to compensate the fallout effect from modifying the η-λ curve. It is also worth noting from the RC slab and beam simulation experiences that the concrete elements interfacing with the rebar are often in a "confined" tension state with a positive (compressive) hydrostatic pressure. In such cases the tension behaviour of these concrete elements are effectively controlled by the b_1 factor rather than b_2, and this adds another layer of consideration in the choice of the b_1 factor (or a similar parameter in other damage-plasticity category of models).

Take the modified η-λ curve with λ_{max}=0.004 as an example, a range of different b_1/b_2 values are examined and results are plotted in **Fig. 19**. Clearly (as obvious from **Eq.2**), the influence of b_1 to the stress-strain response gets larger when the hydrostatic pressure increases, and the stress-strain relation is rather sensitive to the b_1 value under uniaxial compression.

For the intended recommendation of using the exponential η-λ curve with λ_{max}=0.004 and an adjusted b_1=1.2, the corresponding behaviour of the resulting material model under general confined compression is checked and the results are depicted in **Fig. 20**. The comparison with the original KCC model in the confined compression region do not differ significantly, indicating that the recommended modifications for rectifying the tension/shear softening behaviour would not introduce significant side effect when it comes into general compression regime.

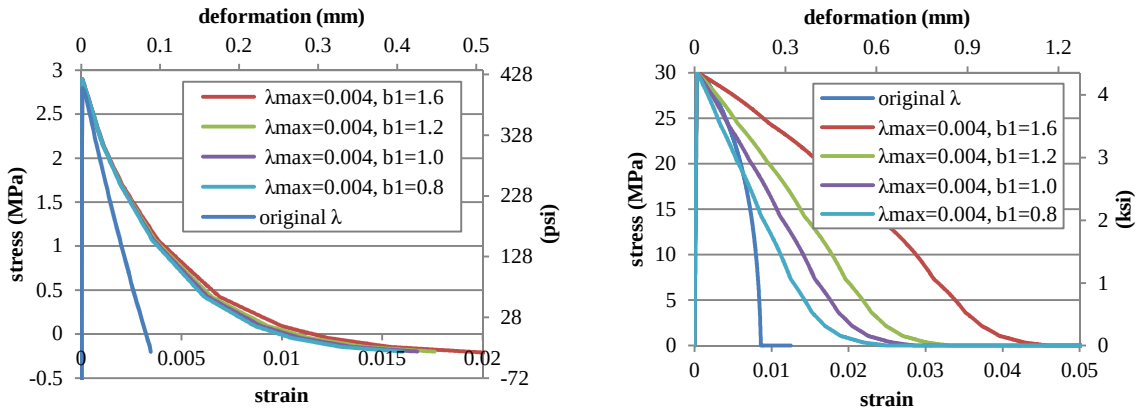

a) confined tension (pressure = 1.5MPa) b) uniaxial compression

*Fig. 19 Influence of b_1 value on stress-strain curves (element size = 25.4mm, 1mm=3.94*10^{-2}in)*

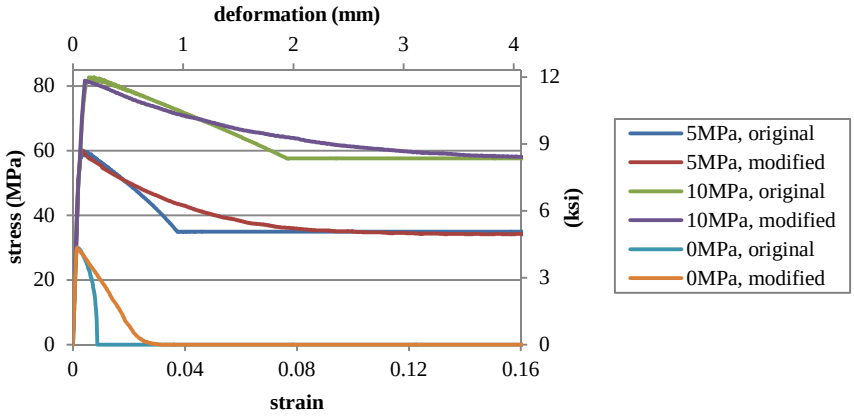

*Fig. 20 Stress-strain curves under confined compression after modification (element size = 25.4mm, 1mm=3.94*10^{-2}in)*

SIMULATION OF THE RC BEAM AND SLAB RESPONSE USING THE MODIFIED KCC MODEL

The parameterisation proposed in previous section has shown to work well in rectifying the tension-softening behaviour while maintaining the original KCC behaviour in general compression regimes. In this section, the modification to KCC model is further varified through the numerical simulation of RC beam and slab response discussed earlier.

Fig. 21 shows the updated load-deflection response for the RC beam using the modified η-λ curve with λ_{max} being 0.004 while b_1 is modified to 1.2. It can be observed that the simulated response using the modified model parameters improve drastically as compared to the original model and the predicted response now agrees satisfactorily with the epxerimental result.

The modified KCC model is also employed to simulate the RC slab response to the blast load described in earlier section. The same modification to the η-λ curve with λ_{max}=0.004 and the seeting of b_1=1.2 is used. **Fig. 22(a)** shows the new deflection response time histories. The simulation results using the modified KCC model again shows a characteristic improvement. The simulated maximum deflection is 113.2mm (4.46in), which is very close to the measured 108.2mm (4.26in). From the damage (crack) patterns presented in **Fig. 22(b)**, it can be seen that with the modified KCC model the abnormal damage along the rebar and in the shear span disappear. The simulated crack distribution is similar to that obtained with the CSC model shown in **Fig. 7**, and both agree favourably with the experimental observations.

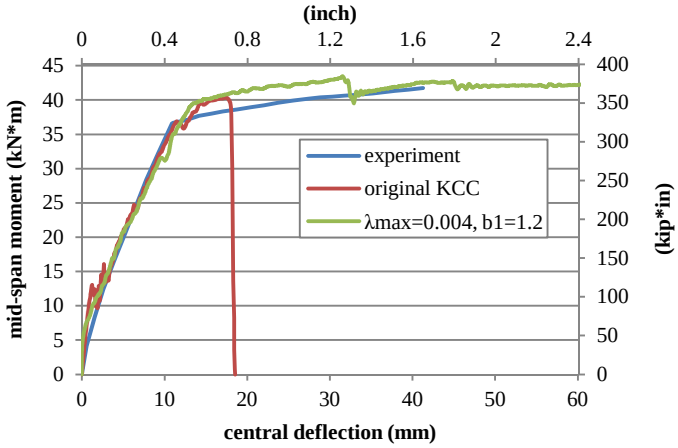

Fig. 21 Central deflection – mid-span moment curves of RC beam under quasi-static load using modified KCC model

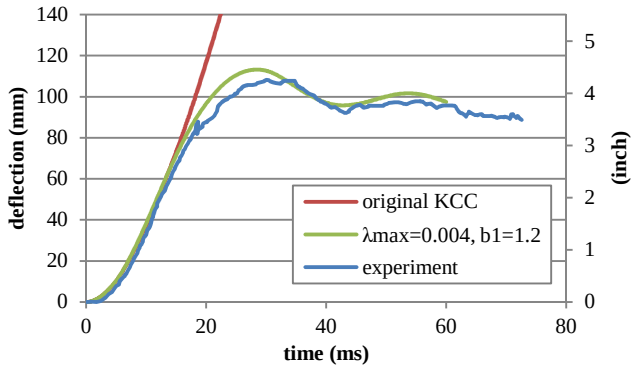

(a) Deflection time history

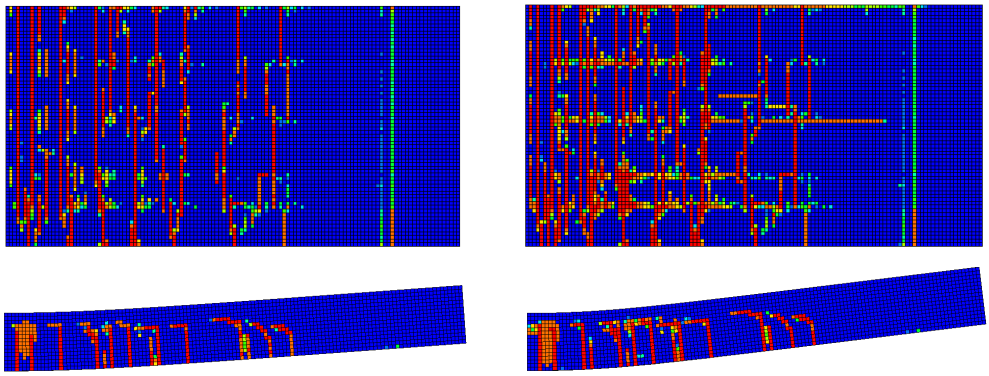

t=10ms t=14ms

(b) Damage pattern (SDF: 1.97~2.00)

Fig. 22 Re-calculated RC slab response to blast load using modified KCC model

From the above analyses it can be generally established that for a general damage-plasticity concrete material model like KCC to extend its satisfactory performance into applications where the response in the relatively low pressure regime may play an important role, an appropriate description of the softening behavioue in shear/tension can be crucial. As far as the KCC model is concerned, a modification to the η-λ curve in conjunction with adequate adjustment of the b_1 factor may suffice, and the recommended setting of the parameters appear to work out fairly satisfactorily in the cases under considerations. Of course, these parameter selections are not expected to be universally suitable, and for specific applications an informed parameter investigation would always be beneficial. However the general trends of the effects of modifying the relevant parameters are expected to hold.

BRIEF DISCUSSION ON THE POTENTIALLY OVER-DUCTILE TENSILE BEHAVIOUR OF CSC MODEL

Generally speaking the performance of the CSC material model in the simulation of the global bending dominated RC slab and beam responses has been satisfactory and no abnormal behaviour due to premature failure of the material has been observed. However, there have been signs of overly ductile response for the material model as evidenced in the RC beam analysis, and particularly in the pull-out simulation shown in **Fig. 16**. The result there tends to indicate that the material model produces an extremely flat softening curve in the bond-slip relation thus greatly overpredicts the ductility of concrete. This raises a question that the CSC model may likely present a problem in the opposite direction of the KCC model.

The results from the single element tests under a uniaxial stress condition, as presented in **Fig. 3**, do not show any apparent over-ductile problem with the CSC model. This suggests that the overly ductile behaviour of the CSC model as evidenced in the RC beam and the pull-out simulation is not simply caused by an inadequate softening rate. Further examination reveals that the problem would arise when a certain level of pressure is involved. This is elaborated in what follows.

In CSC model, in addition to the definition of the confinement (pressure) dependent failure surface, an extra equation is introduced to factor down the maximum possible damage level in the ductile or compressive situations:

$$d_{\max} = \begin{cases} \left(\dfrac{\sqrt{3J_2}}{I_1}\right)^{1.5} & \text{for} \quad \dfrac{\sqrt{3J_2}}{I_1} < 1 \\ 0.999 & \text{otherwise} \end{cases} \tag{13}$$

The non-dimensional term in parentheses is a stress invariant ratio that is made equal to 1 in unconfined compression and less than 1 under confined compression. This effect may be illustrated in **Fig. 23**, and it is activated only when the stress condition falls into the shadowed area. The power of 1.5 is set in the default model.

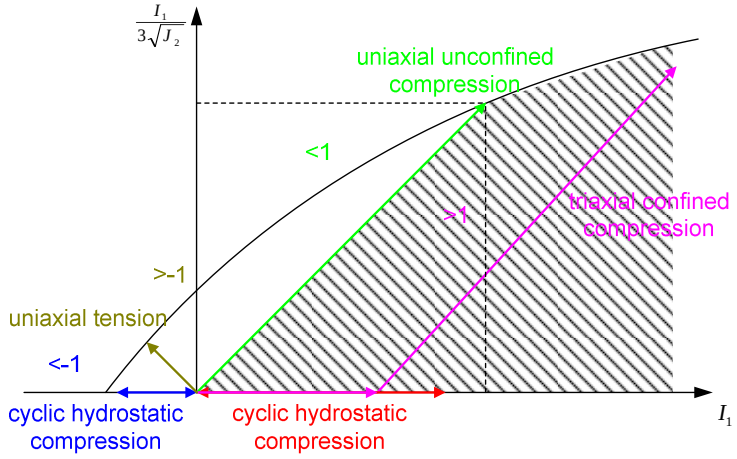

Fig. 23 Different stress paths and correspondent stress invariant ratios

However in the case of confined tension ($0 < I_1/\sqrt{3J_2} < 1$), the above CSC implementation of confinement effect becomes problematic, which can be demonstrated by a single element stress tests illustrated in **Fig. 24**. As can be observed, in the softening regime a fully damaged state can never be reached in the CSC if the element is under a hydrostatic pressure condition, even with a small confinement of just 0.2 MPa. When the pressure increases, the material becomes more ductile. With a confinement of 3MPa, the stress-strain response becomes extremely flat and the material acts almost like elasto-plastic.

An examination of the stress paths illustrated in **Fig. 24b** shows that the stress starts to decrease through the original path once it meets the tensile meridian; however due to reduced maximum possible damage level, the stress is always prevented from unloading across to the right side of the straight line of $I_1 = \sqrt{3J_2}$, thus the strength is restrained and never deteriorates to a zero stress state. The persist existence of a minimum stress state may not be of a problem by itself; however, such mechanism of consideration of the confinement effect by an

extra reduction to the damage index can cause unrealistic over-ductile tensile response when an appreciable level of pressure (e.g. 2~3 MPa) is present, which can become problematic. Although a detailed investigation of the CSC model is beyond the scope of the present paper, the above phenomenon is deemed to be worth noting while the general behaviour of the material model proves to be satisfactory in a flexure dominated response scenario.

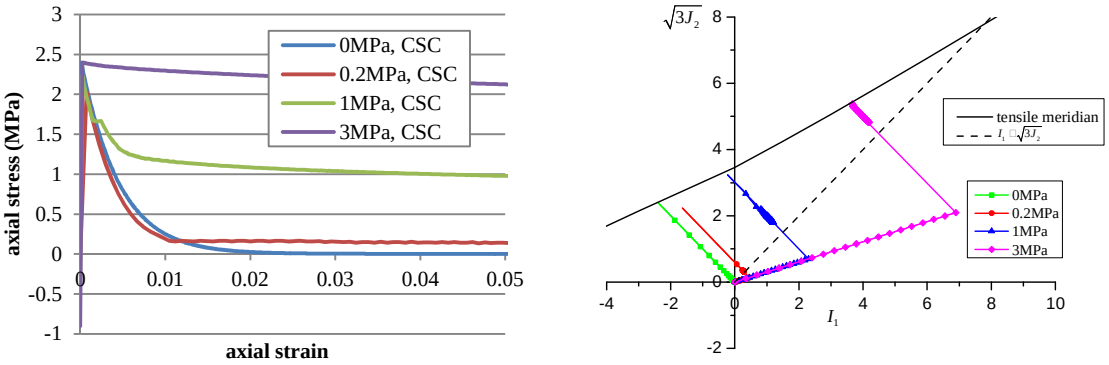

(a) Stress-strain curves under confined tension (b) Graphical explanation of the stress paths

Fig. 24 Behaviour of CSC material model under confined tension (1MPa=145psi)

CONCLUSIONS

Numerical simulation of reinforced concrete structures under impact and blast loadings requires the material models to be able to accommodate a wide range of stress, strain rate and deformation conditions. Although extensive calibration and validation studies have been conducted for typical concrete material models under a variety of loading conditions, the performance and demands of the material models in a reinforced concrete environment and under a global deformation dominated response regime is relatively less explored. The present study examined the performance of KCC model in comparison with the CSC model in the application of RC slab and beams for impact and blast loading.

The simulation on the blast response of the RC slab demonstrates that with the default KCC model the simulated response tends to fail prematurely due to a rapid loss of the shear and tensile strength of concrete, particularly in the elements to which the reinforcing bars are attached. Further simulation on an RC beam under a quasi-static loading shows a similar phenomenon. An examination of the model behaviour in a classical pull-out scenario confirms that without a more gradual softening stage the premature failure mode due to loss of rebar-concrete interactions tends to be inevitable.

Rectification of this model problem is then focused on realising a more gradual softening (descending) phase of the tensile and shear behaviour, including in the conditions where an appreciable hydrostatic pressure is involved. The proposed modification includes a modified damage function, i.e. the η-λ curve, as well as an adjustment of the plastic strain accumulation factor b_1 of KCC model. With the proposed modification, the KCC model is found to behave rather satisfactorily in modelling the RC slab and beam responses under blast and quasi-static load situations.

It should be noted that the proposed modification on KCC model is aimed at alleviating the brittleness in the tension-softening regime, while keeping the model behaviour in other general stress conditions largely unaffected. In this way the general validation of the material model as observed in the literature still holds with the modification. Certainly under a wider range of blast and other loading conditions the effect of the modification will need to be checked more comprehensively and this is part of an extended investigation which is currently ongoing.

Generally speaking the CSC model behaves quite satisfactorily in the simulations of the response of RC components dominated by global bending deformations. Further examination of the model performance reveals that CSC model is inclined towards the opposite direction of KCC model in a tension or shear dominated response regime, especially when a limited amount of confining pressure is involved; in such conditions it tends to be excessively ductile. The cause of this abnormal phenomenon is deemed to originate from the use of a reduction of damage in a confined stress condition. Such a phenomenon has not been well calibrated in the literature, and should be treated with care before an appropriate resolution is available.

REFERENCES

1. Bischoff, P. H., and S. H. Perry. "Compressive behaviour of concrete at high strain rates." *Materials and structures* 24.6 (1991): 425-450.
2. Donze, F. V., S-A. Magnier, L. Daudeville, C. Mariotti, and L. Davenne. "Numerical study of compressive behavior of concrete at high strain rates." *Journal of engineering mechanics* 125.10 (1999): 1154-1163.
3. Li, Q. M., and Meng, H., "About the dynamic strength enhancement of concrete-like materials in a split Hopkinson pressure bar test." *International Journal of Solids and Structures* 40.2 (2003): 343-360.
4. Song, Z., and Lu Y., "Mesoscopic analysis of concrete under excessively high strain rate compression and implications on interpretation of test data." *International Journal of Impact Engineering* 46 (2012): 41-55.
5. Polanco-Loria, M., Hopperstad, O. S., Børvik, T., and Berstad, T., "Numerical predictions of ballistic limits for concrete slabs using a modified version of the HJC concrete model." *International Journal of Impact Engineering* 35, no. 5 (2008): 290-303.
6. Unosson, M., and Nilsson, L., "Projectile penetration and perforation of high performance concrete: experimental results and macroscopic modelling." *International journal of impact engineering* 32.7 (2006): 1068-1085.
7. Tu Z. and Lu Y., "Evaluation of typical concrete material models used in hydrocodes for high dynamic response simulations, " *International Journal of Impact Engineering* 2009;36(1):132–46.
8. Zakrisson, B., Wikman, B., and Häggblad, H. Å., "Numerical simulations of blast loads and structural deformation from near-field explosions in air." *International Journal of Impact Engineering* 38.7 (2011): 597-612.
9. LSTC, LS-DYNA Keyword User's Manual. Version 971, Livermore, California, 2012.
10. Malvar L.J. and Crawford J.E., "A plasticity concrete material model for DYNA3D," *International Journal of Impact Engineering* 1997;19(97):847–73.
11. Murray Y. D., Users Manual For LS-DYNA Concrete Material Model 159. Publication No. FHWA-HRT-05-062, Federal Highway Administration, McLean, VA, 2007.
12. Crawford J.E., Wu Y., Choi H., Magallanes J.M. and Lan S., Use and Validation of the Release III K&C Concrete Material Model in LS-DYNA, Technical Report TR-11-36.5, Karagozian & Case, Glendale, CA, 2012.
13. Magallanes J.M., Wu Y., Malvar L.J. and Crawford J.E., "Recent improvements to release III of the K&C concrete model," *Eleventh International LS-DYNA Users Conference*, 2010, pp.37–48.
14. Malvar L.J., Crawford J.E. and Morrill K.B., "K&C concrete material model release III--Automated generation of material model input," Technical Report TR-99-24.3, Karagozian & Case, 2000.
15. Schwer L.E. and Malvar L.J., "Simplified concrete modeling with *MAT_CONCRET_DAMAGE_REL3," *LS-DYNA Anwenderforum*, Bamberg, 2005, pp.49–60.
16. Tu Z. and Lu Y., "Modifications of RHT material model for improved numerical simulation of dynamic response of concrete, " *International Journal of Impact Engineering* 2010;37(10):1072–82.
17. ARUP, Verification of the Karagozian and Case Material-Model for LS-DYNA 971 R3 Report. 2009.
18. Magallanes J.M., "Importance of concrete material characterization and modelling to predicting the response of structures to shock and impact loading," *10th International Conference on Structures Under Shock and Impact*, Southampton, UK, 2008, pp.241–50.
19. Wu Y., Crawford J.E. and Magallanes J.M., "Performance of LS-DYNA® concrete constitutive models," *12th International LS-DYNA Users Conference*, Dearborn, Michigan, US, 2012, pp.1–14.
20. Bažant, Zdeněk P., and Byung H. Oh. "Crack band theory for fracture of concrete." *Matériaux et construction* 16.3 (1983): 155-177.
21. Comité euro-international du béton, CEB-FIP Model Code 1990. FIB-Féd. Int. du Béton; 1993.
22. University of Missouri-Kansas City, Blast Blind Simulation Contest. http://sce.umkc.edu/blast-prediction-contest/ 2013.
23. Xu J. and Lu Y., "A comparative study of modelling RC slab response to blast loading with two typical concrete material models," *International Journal of Protective Structures* 2013;4(3):415–32.
24. Thiagarajan G., "2012 Blast Blind Prediction Results - Overview Of Methods Used And Observations," *ACI Fall 2013 Convention: Blast Blind Predict of Response of Concrete Slabs Subjected to Blast Loading*, Phoenix, Arizona, US, 2013.
25. Janney J.R., Hognestad E. and McHenry D., "Ultimate flexural strength of prestressed and conventionally reinforced conrete beams," *Journal of the American Concrete Institute Proceedings* 1956; 52(1):601.
26. Eligehausen R., Popov E.P. and Bertero V., "Local bond stress-slip relationships of deformed bars under generalized excitations. UCB/EERC-83/23, Earthquake Engineering Research Center, Berkeley; 1983.
27. Eligehausen R., Popov E.P. and Bertero V., "Local bond stress-slip relationships of deformed bars under generalized excitations," *Proceedings of the 7th European Conference on Earthquake Engineering*. Vol. 4., Athens : Techn. Chamber of Greece,, 1982, pp.69–80.